PHYSICAL REVIEW B **82**, 121303(R) (2010)

# Thresholdless coherent light scattering from subband polaritons in a strongly coupled microcavity

Johannes Gambari,[1] Antonio I. Fernandez-Dominguez,[1] Stefan A. Maier,[1] Ben S. Williams,[2,3] Sushil Kumar,[3] John L. Reno,[4] Qing Hu,[3] and Chris C. Phillips[1]

[1]*Physics Department, Imperial College London, London SW7 2AZ, United Kingdom*

[2]*Department of Electrical Engineering, California NanoSystems Institute, University of California, Los Angeles, California 90095, USA*

[3]*Department of Electrical Engineering, Computer Science and Research Laboratory of Electronics, Massachusetts Institute of Technology, Cambridge, Massachusetts 02139, USA*

[4]*Sandia National Laboratories, Department 1123, MS 0601, Albuquerque, New Mexico 87185-0601, USA*

(Received 23 July 2010; published 9 September 2010)

We study a "strongly coupled" (SC) polariton system formed between the atomlike intersubband transitions in a semiconductor nanostructure and the terahertz optical modes that are localized at the edges of a gold aperture. The polaritons can be excited optically, by incoherent excitation with band-gap radiation, and we find that they also coherently scatter the same input laser, to give strikingly sharp "sideband" (SB) spectral peaks, in the backscattered spectrum. The SB intensity is a sensitive track of the polariton density and they can be detected down to a quantum noise floor that is more than 2500 times lower than the excitation thresholds of comparable quantum cascade laser diodes. Compared with other coherent scattering mechanisms, higher-order SB scattering events are readily observable, and we speculate that if suitably optimized, the effect may find utility in a passive component capable of all-optical wavelength shifting for telecommunications systems.

DOI: 10.1103/PhysRevB.82.121303 PACS number(s): 78.67.Pt

In a strongly coupled (SC) system, the electronic transitions are so strongly coupled to the photon modes that they form a new hybrid entity, a polariton, where the coupling strength is characterized by a vacuum-Rabi energy, $\hbar\Omega_{\mathrm{VR}}$, that exceeds the original natural linewidths of both the electronic transitions and the photon modes. Viewed in the time domain, the excitation energy cycles coherently, at a rate $\Omega_{\mathrm{VR}}^{-1}$ between electronic and photonic forms, before being lost, either by optical emission or by other nonradiative loss channels.[1]

Here we study a SC system whose polaritons are formed from the terahertz (THz) photon modes of a tightly confined metal-semiconductor microcavity. These photon modes hybridize with the electronic "intersubband transitions" (ISBTs) in a semiconductor nanostructure. The resulting polaritons are excited incoherently, using interband excitation with a near-IR (NIR) laser $\omega_{\mathrm{NIR}}$ (Fig. 1), to excite electrons high into the conduction band, whence they scatter down through the subband structure until they reach the polariton state formed between the $|2\rangle \Rightarrow |1\rangle$ and the THz optical modes. Because the polaritons carry an optical dipole, and we find that they coherently scatter that same input beam, generating strikingly sharp, multiple-order sidebands (SBs), at $\omega_{\mathrm{SB}} = \omega_{\mathrm{NIR}} + n\omega_{\mathrm{THz}}$ $(n=-2,-1,0,+1+2)$ in the backscattered spectrum.

The devices studied were fabricated from epilayers comprising many (~175) repeats[2,3] of a GaAs/[Al,GaAs] semiconductor nanostructure module (Fig. 1). The epilayers were fabricated into ~10-$\mu$m-thick gold-epilayer-gold sandwich waveguides that were able[4,5] to confine the THz fields into layers ~10 times thinner than the $\lambda \sim 100$ $\mu$m free-space wavelength. Three device structures were studied, identified as "$\lambda \sim 80$ $\mu$m,"[3] "$\lambda \sim 100$ $\mu$m,"[2] and "$\lambda \sim 120$ $\mu$m"[3] according to the free-space wavelengths they emitted when they were electrically driven, in separate experiments,[2,3] as standard quantum cascade lasers (QCLs).

Each period of the $\lambda \sim 100$ $\mu$m nanostructure in Fig. 1 comprises[2] **4.9**/7.9/**2.5**/6.6/**4.1**/15.6/**3.3**/9.0-nm-thick layers of $\mathbf{Al_{0.3}Ga_{0.7}As}$/GaAs and supports ~5 confined electron states. The 15.6 nm well is doped at $1.9 \times 10^{16}$ cm$^{-3}$, giving an areal electron density, $n_s = 3 \times 10^{10}$ cm$^{-2}$ and a Fermi energy of ~1 meV, so only the lowest subband is occupied at equilibrium.[6]

The $|2\rangle \Rightarrow |1\rangle$ ISBT had a modeled energy of $E_{12} = 15.8$ meV and a transition dipole of $z_{12} = 2.3$ nm. The epilayer was fabricated into a metal-semiconductor-metal waveguide that was ~10 $\mu$m $\times$ 50 $\mu$m $\times$ 834 $\mu$m long, with a periodic array (Fig. 1) of six 30 $\mu$m $\times$ 8 $\mu$m slots, spaced by $\Lambda = 31$ $\mu$m, etched into its top surface.

The devices were illuminated normally (Fig. 1), with a tunable continuous-wave titanium:sapphire near-infrared laser, $\omega_{\mathrm{NIR}}$, with a 50 $\mu$m spot size and a linewidth $\Delta\omega_{\mathrm{NIR}} < 0.1$ meV. The backscattered light was polarization filtered before being analyzed with a 0.25 m grating monochromator and a standard, background subtracting, photon-counting setup whose cooled photomultiplier had a dark count <10 counts/s. The sharpness of the SBs meant careful attention to the system's mechanical and laser wavelength stability was needed to see them.

As well as the elastically scattered light, the backscattered spectra featured a $\lambda = 815$ nm/1.52 eV band-gap photoluminescence peak (not shown) but the sharpness of the SB peaks made it easy to fit and subtract these background signals numerically. The optical collection efficiency was calibrated to allow the SB powers emitted by the sample to be obtained to an estimated accuracy of 20%. The data presented in Figs. 1–3 were taken at low spectral resolution to improve the signal-to-noise ratio, high-resolution runs (not shown) always found resolution-limited SB linewidths, down to the spectrometers' 0.3 nm/0.5 meV working limit. For a given device, the SB features stayed at a fixed frequency interval from $\omega_{\mathrm{NIR}}$, as the Ti:sapphire laser was tuned over a wide wavelength range (Fig. 2).

 

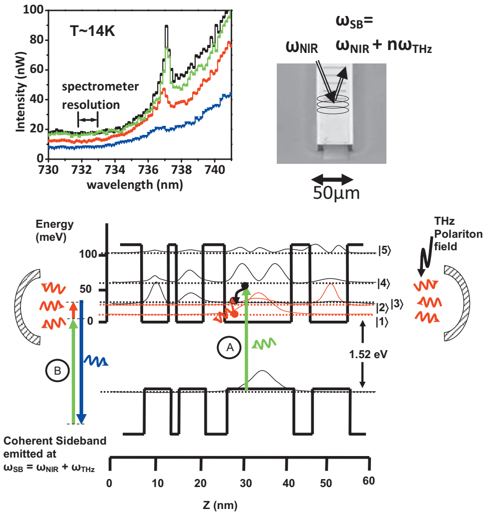


FIG. 1. (Color) A single period of the nanostructure, embedded in a THz microcavity which is symbolized here by external mirrors. THz polaritons are created (a) by photocarriers, excited by a near-IR laser, $\omega_{NIR}$, cascading down through the subband system until they reach the polariton state formed between the $|2\rangle \Rightarrow |1\rangle$ ISBT and the THz optical modes. The same near-IR laser (b) is also coherently scattered from these $\omega_{THz}$ polaritons and generates sidebands at $\omega_{SB}=\omega_{NIR}+n\omega_{THz}$. Upper left inset: raw spectra of the light backscattered from the top of the device, as the $\sim$50 $\mu$m diameter $\lambda \sim 744$ nm $\omega_{NIR}$ laser spot is scanned along the center of the ridge, across one of its slots (upper right inset), at distances from the center of the slot of 0 $\mu$m (black squares), 20 $\mu$m (green triangles), 40 $\mu$m (red circles), and 100 $\mu$m (blue inverted triangles).

All the SBs disappeared if $\hbar\omega_{NIR}$ was tuned below the $\sim$1.52 eV/815 nm effective band gap of the nanostructure. Both first- and second-order peaks vanished [Fig. 3(b)] by $\sim$120 K, similar to the maximum operation temperature of comparable QCLs.[3] The optical polarization of the SBs matched the polarization of the $\omega_{NIR}$ input to better than 99%, whether it was linear or circular.

Biasing the waveguide allowed it to be used as a photoconductive detector to measure the fraction of the $\omega_{NIR}$ beam that made it through the illuminated slot in the top gold layer. When the laser spot was scanned along the center of the waveguide, across a given slot (Fig. 1 inset) the SB intensity scaled with this photocurrent.

The SBs were reproducible over months of measurement and through numerous changes to the optical setup. They were never seen in control experiments, when the $\omega_{NIR}$ spot was focused onto (i) unmetallized epilayer samples, (ii) onto GaAs test wafers, (iii) onto highly scattering parts of the cryostat mount, or (iv) onto the gold contacting layers adjacent to the slots in the structure of Fig. 1.

The way the SBs tune with $\omega_{NIR}$ [Figs. 2(b) and 2(c)] immediately implies that they are generated by a form of coherent scattering. We rule out normal phonon Raman scattering because the SBs are $\sim$100$\times$ more intense, at least 12 times sharper, and appear at the wrong energy offsets [Fig. 3(a)] compared with typical LO phonon Raman lines.

Coherent scattering processes generate SBs whose line shape is a convolution of the linewidths of the input laser

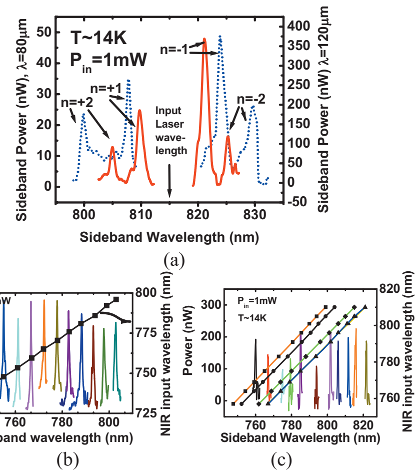


FIG. 2. (Color) (a) Background-subtracted spectra taken, from the $\lambda \sim 120$ $\mu$m (red solid line, right-hand vertical axis), and $\lambda \sim 80$ $\mu$m (blue dotted line, left-hand vertical axis) devices, both showing coherent sidebands at $\omega_{SB}=\omega_{NIR}+n\omega_{THz}$. ($n=-2,-1,+1,+2$), with resolution-limited ($\Delta\lambda \sim 1.4$ nm here) linewidths. (b) Tuning behavior (right-hand axis) and $n=1$ sideband spectra (left-hand axis) of the $\lambda \sim 100$ $\mu$m structure as the near-IR input wavelength (1 mW power) is scanned. (c) Tuning behavior (right-hand axis) of the $n=+2$ (orange squares), $n=+1$ (black circles), $n=-1$ (green diamonds), and $n=-2$ (blue triangles) SB peaks from the $\lambda \sim 80$ $\mu$m structure. Spectra (left-hand axis), of the $n=-2$ SBs peaks from the same sample at the input wavelength denoted by the corresponding blue triangle data point on the tuning line.

($<$0.1 meV) and that of the scattering excitation. Therefore, the sharpness of the SB lines ($<$0.5 meV) compared with an estimated bare ISBT linewidth of approximately a millielectron volt[7] argues that they cannot be due to standard electronic Raman scattering from the ISBT.

SB have previously been generated by exploiting optical frequency mixing effects which arise due to nonlinear components of the optical polarizability in the material of a QCL.[8,9] However, this mechanism requires the presence of a spectrally sharp THz optical field inside the structure and this could only be happening here if we had somehow managed to produce an optically pumped analog of a standard QCL. This possibility, however, is strongly at odds with the fact that we see no excitation threshold for the onset of the SB generation. Defining the SB generation efficiency, $\eta_{SB}$, as the ratio between the detected sideband intensity and the $\omega_{NIR}$ power entering the slot [Fig. 3(c)], $\eta_{SB}$ climbs linearly from the detector system's photon noise floor as the $\omega_{NIR}$ pump power is increased. When the $\lambda \sim 100$ $\mu$m device of Fig. 1 was configured as a QCL,[2] its threshold current density, $J_{th}$ $\sim$435 A cm$^{-2}$, corresponded to $\sim 4.8 \times 10^{27}$ s$^{-1}$ m$^{-2}$ ISBT transitions throughout the epilayer's 175 periods. In our optical experiments (Fig. 3) the SB first appears with $\sim$0.1 mW entering the $2.4 \times 10^{-10}$ m$^2$ slot, i.e., an areal excitation rate, $\sim 1.7 \times 10^{24}$ s$^{-1}$ m$^{-2}$, that is $\sim$2500 times smaller than the comparable QCL threshold. Finally, the ease with which the $n=\pm 2$ higher-order processes are seen [Fig. 2(a)] contrasts sharply with what is observed in Raman and nonlinear frequency mixing experiments.

To understand the origin of the sidebands we first need to

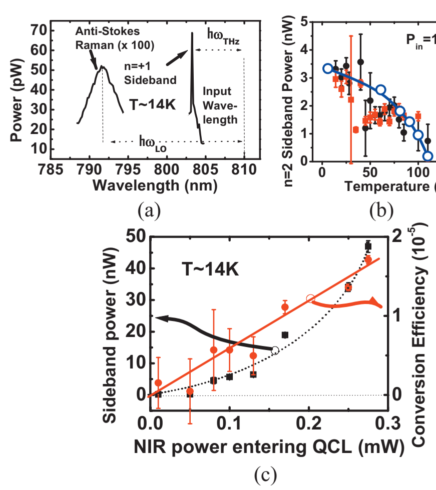


FIG. 3. (Color) (a) Comparison between the anti-Stokes GaAs Raman line (enhanced by $\times 100$ on this plot) and a typical $n=+1$ SB. (b) Temperature dependence of the SB intensity with a $\sim 1$ mW $\lambda \sim 810$ nm input beam the $\lambda \sim 80$ $\mu$m device; red squares, the $n=-1$ SB intensity (right-hand axis), black filled circles, the $n=-2$ SB intensity (left-hand axis); open blue circles, output of a QCL made from the same heterostructure (Ref. 3) (arbitrary units). (c) SB power (black squares, left-hand axis) and conversion efficiency (red circles, right-hand axis) from the $\lambda \sim 100$ $\mu$m device of Fig. 1. The dashed (solid) lines are guides to the eye, evidencing the quadratic (linear) dependencies of the power (efficiency) at low NIR pump levels

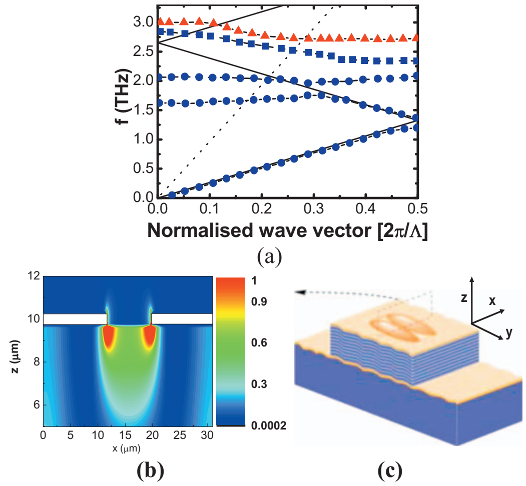


FIG. 4. (Color) (a) THz photon modes supported by the device of Fig. 1, which is modeled as a superlattice array of slots on the top of an infinite (in $x$) ridge wave guide. Modes are enumerated in terms of the superlattice wave vector, $2\pi/\Lambda$, where $\Lambda=31$ $\mu$m is the slot spacing. Blue squares, the radiating mode designed to outcouple radiation when electrically driven as a QCL. Red triangles: the localized family of modes. Dotted (solid) lines are light lines in the vacuum (semiconductor). (b) Energy distribution, across a single slot in the periodic structure, of the localized modes. (c) Schematic three-dimensional distribution of the fields in the localized mode concentrated at the edges of the slots in the structure.

estimate the coupling between the ISBTs and the THz photon modes. The ISBT energy is independent of electron in-plane wave vector, so strong electron correlation effects[10] concentrate all the oscillator strength into a single, dispersionless, atomlike Lorentzian line, with all electrons simultaneously coupling to the photon modes in the same way. Coupled with the large transition dipole, $z_{12}$, this has already been shown, in planar structures, to generate SC with giant $\hbar\Omega_{VR}$ energies,[11,12] especially with the wider wells used in THz devices.[13] In fact, $\hbar\Omega_{VR}$ values have been achieved that not only exceed the linewidths, but are also comparable with the transition energy itself,[14,15] the so-called ultraSC (USC) condition,[16]

In our nonplanar devices, the photon modes are confined in all three dimensions, so their mode shapes and volumes must be calculated numerically. We use a standard finite-difference time-domain (FDTD) method, on a 125 nm mesh, which treats the gold as a perfect conductor and the semiconductor as an insulator with a dielectric constant of 13.3.[17] It models the ridge structure of Fig. 1 as an infinite array of slots and uses periodic boundary conditions to allow the modes to be plotted in terms of the superlattice wave vectors, $2\pi/\Lambda$, where $\Lambda=31$ $\mu$m is the slot repeat distance (Fig. 4).

The model correctly reproduces the "radiating" modes [Fig. 4(a) blue squares] that the slot array was designed to support so as to outcouple[4] the THz radiation when biased as a QCL. However, at almost the same energy (12.5 meV/$\sim 3$ THz) there is another family of "localized" THz modes [Fig. 4(a) red triangles] whose field distributions are tightly localized at the slot edges, similar to the ultraconfined modes recently reported[18,19] in other subwavelength structures. These originate from a vertical $\frac{1}{4}$ wave "organ-pipe" resonance, with a node at the lower gold layer and an antinode at the slot opening, so they resonate roughly corresponding to a free-space wavelength $\lambda \sim 4nh$, where $n$ is the semiconductor refractive index and $h \sim 10$ $\mu$m the slab thickness. The field localization means that photon modes on adjacent slots oscillate almost independently, so they are practically monoenergetic and dispersionless in the photonic superlattice plot [Fig. 4(a)]. The result is that all the THz modes in this family can strongly couple to the electronic ISBTs at the same time. This is in marked contrast to what happens in dispersive two-dimensional systems,[11–15] where only a subset of the traveling-wave photon modes couple to the ISBTs and the anticrossing behavior can be mapped out directly in spectroscopic studies. The field localization around the slot edge also gives very weak out coupling to the free-space THz modes, raising the $Q$ factor to $\sim 1100$, compared with $\sim 57$ for the radiating modes.

The computed volume of the localized mode, $V \sim 496$ $(\mu\text{m})^3$, is only $\sim \lambda^3/2000$ of the $\lambda \sim 100$ $\mu$m free-space wavelength and $\sim 1/50$ of $\lambda^3$ in the semiconductor material. Its frequency resonates closely with the modeled $E_{12} \sim 15$ meV (Fig. 1) ISBT energy and its electric field is mainly vertically polarized, so it couples strongly to the vertically polarized $z_{12}$ of the ISBT. Also, its half-height energy density [Fig. 4(b)] is only $\sim 0.96$ $\mu$m below the semiconductor-air interface, so overlaps well with the $\sim 1$ $\mu$m penetration depth of the $\omega_{NIR}$ incoherent pump light from the Ti:sapphire laser.[17]

We compute $\hbar\Omega_{VR}$ for the localized photon mode by equating the classical stored electromagnetic energy, $V\varepsilon_r\varepsilon_0 E_{vac}^2$, with the quantum photon ground-state energy, $\hbar\omega_{THz}/2$, to give a mean zero-point vacuum field of $E \sim 142$ V m$^{-1}$ for $\hbar\omega_{THz}=15$ meV. A single-electron ISBT oscillator will couple to this field to give $\hbar\Omega_{VR}=2Ee\ z_{12}$, which, with $\varepsilon_r=13.3$ (Ref. 17) and $z_{12}\sim 2.3$ nm gives $6.3\times 10^{-7}$ eV. A factor $f=0.92$ of the mode energy lies inside the semiconductor, and $N\sim 2.4\times 10^6$ ISBT electrons lies within this volume, giving a total coupling energy of $\hbar\Omega_{VR}=2Ee\ z_{12}\ N^{1/2}\sim 1.0$ meV. Even with no photoexcitation this is some ~7% of the ISBT energy and will increase further under the experimental conditions. Assuming, e.g., an interband carrier recombination time of ~1 ns, ~1 mW of absorbed laser power would triple the local electron concentration and increase $\hbar\Omega_{VR}$ by $\sim\sqrt{3}$.

This $\hbar\Omega_{VR}$ value exceeds both the <0.5 meV upper bound to the linewidth of the excitation responsible for the SB generation and the ~15 $\mu$eV modeled linewidth of the localized photon mode. This confirms the SC nature of the electron-photon system, i.e., the SBs arise from coherent scattering mechanism from polaritons whose linewidths lie between[7] the approximately one millielectron volt ISBT linewidth and the ~15 $\mu$eV localized photon mode linewidth.

At higher optical excitation levels (not shown), the $\lambda \sim 100$ $\mu$m device $n=1$ SB conversion efficiency peaks at $\sim 5\times 10^{-5}$ (at ~1 mW input power), and then drops, most likely due to a combination of sample heating [Fig. 3(b)] and, at >3 mW, the carrier concentration rising high enough to start populating the second subband.

There are strong parallels between this SC system, and previous atom-cavity studies,[20] where coherent output radiation was seen without the system needing to be driven into population inversion. Unfortunately, our attempts to detect the emitted optical component of the THz polaritons directly (i.e., to demonstrate a THz analog of a so-called "inversionless laser") were frustrated by the poor sensitivity of current THz detectors, and the very weak coupling of the localized modes to the outside world.

That said, we believe that this effect may prove more useful as a simple, passive coherent optical mixing device than as a source of THz radiation. Although the conversion efficiencies and operating temperatures are low at the moment, this effect still has potential for frequency shifting, e.g., an optical bit stream by a fixed frequency interval that can be tightly specified at the design stage and would be data transparent and operate across the full optical telecommunications bandwidth. Moving to the [In,Al,Ga],As materials system and optimizing $\hbar\Omega_{VR}$ by judicious choice of doping levels, THz mode shapes and ISBT $z_{12}$ values may move the operating wavelengths, temperatures, and efficiencies toward technologically useful values.

Helpful conversations with Paul Eastham are gratefully acknowledged. This work was supported by the Engineering and Physical Sciences Research Council (EPSRC), and by the U.S. Air Force Office of Scientific Research (AFOSR).

[1] M. S. Skolnick, T. A. Fisher, and D. M. Whittaker, Semicond. Sci. Technol. **13**, 645 (1998).

[2] B. S. Williams, S. Kumar, Q. Hu, and J. L. Reno, Opt. Express **13**, 3331 (2005).

[3] B. S. Williams, S. Kumar, Q. Qin, Q. Hu, and J. L. Reno, Appl. Phys. Lett. **88**, 261101 (2006).

[4] S. Kumar, B. S. Williams, Q. Qin, A. W. M. Lee, and Q. Hu, Opt. Express **15**, 113 (2007).

[5] S. A. Maier, Opt. Express **14**, 1957 (2006).

[6] When optically pumped, the subband populations are partly determined by the electron intersubband scattering rates, but these are much faster than typical approximately nanosecond interband recombination times, so the majority of the electrons will always be in the lowest subband at $T\sim 14$ K and the ~1 mW excitation levels used for most of this study. Depending on assumptions made about the interband recombination time, it is possible that carrier redistribution effects may be contributing to the higher temperature portion ($T>90$ K) of Fig. 3(b).

[7] Electroluminescence spectra from test diodes had ~4 meV linewidths but these came from "diagonal" ISBTs with strong interface broadening arising from the high electric fields needed for the measurements. ~2 meV ISBT linewidths were seen in reflectance measurements of planar samples with similar (3.7 THz) ISBT energies to the device of Fig. 1 (Ref. 13).

[8] S. S. Dhillon, C. Sirtori, S. Barbieri, A. de Rossi, M. Calligaro, H. E. Beere, and D. A. Ritchie, Appl. Phys. Lett. **87**, 071101 (2005).

[9] C. Zervos *et al.*, Appl. Phys. Lett. **89**, 183507 (2006).

[10] D. E. Nikonov, A. Imamoglu, L. V. Butov, and H. Schmidt, Phys. Rev. Lett. **79**, 4633 (1997).

[11] D. Dini, R. Köhler, A. Tredicucci, G. Biasiol, and L. Sorba, Phys. Rev. Lett. **90**, 116401 (2003).

[12] E. Dupont, H. C. Liu, S. Schmidt, and A. Seilmeier, Appl. Phys. Lett. **79**, 4295 (2001).

[13] Y. Todorov, A. M. Andrews, I. Sagnes, R. Colombelli, P. Klang, G. Strasser, and C. Sirtori, Phys. Rev. Lett. **102**, 186402 (2009).

[14] A. A. Anappara, A. Tredicucci, F. Beltram, G. Biasol, L. Sorba, S. de Liberato and C. Ciuti, Appl. Phys. Lett. **91**, 231118 (2007).

[15] J. Plumridge, E. Clarke, R. Murray, and C. Phillips, Solid State Commun. **146**, 406 (2008).

[16] C. Ciuti, G. Bastard, and I. Carusotto, Phys. Rev. B **72**, 115303 (2005).

[17] From the point of view of interband absorption and dielectric response, the heterostructure slab region closely approximated $n\sim 5\times 10^{15}$ cm$^{-3}$ bulk GaAs, with absorption properties as described in J. S. Blakemore, J. Appl. Phys. **53**, R123 (1982).

[18] M. A. Seo, H. R. Park, S. M. Koo, D. J. Park, J. H. Kang, O. K. Suwal, S. S. Choi, P. C. M. Planken, G. S. Park, N. K. Park, Q. H. Park, and D. S. Kim, Nat. Photonics **3**, 152 (2009).

[19] R. F. Oulton, V. J. Sorger, T. Zentgraf, R.-M. Ma, C. Gladden, L. Dai, G. Bartal, and X. Zhang, Nature (London) **461**, 629 (2009).

[20] J. McKeever, A. Boca, A. D. Boozer, J. R. Buck, and H. J. Kimble, Nature (London) **425**, 268 (2003).